

---

RESEARCH ARTICLE

---

# The Influence of Early Measurements Onto the Estimated Kidney Dose in [ $^{177}\text{Lu}$ ][DOTA<sup>0</sup>,Tyr<sup>3</sup>] Octreotate Peptide Receptor Radiotherapy of Neuroendocrine Tumors

Andreas Delker, Harun Ilhan, Christian Zach, Julia Brosch, Franz Josef Gildehaus, Sebastian Lehner, Peter Bartenstein, Guido Böning

*Department of Nuclear Medicine, University Hospital, Ludwig-Maximilians-Universität, Munich, Germany*

---

## Abstract

**Purpose:** Multiple measurements have been required to estimate the radiation dose to the kidneys resulting from [ $^{177}\text{Lu}$ ]DOTATATE therapy for neuroendocrine tumors. The aim of this study was to investigate the influence of early time-point measurement in the renal dose calculation.

**Procedures:** Anterior/posterior whole-body planar scintigraphy images were acquired at approx. 1, 24, 48, and 72 h after administration of [ $^{177}\text{Lu}$ ]DOTATATE. Furthermore, we acquired planar 1-bed dynamic recordings in 12 frames (5 min each) during the first hour. We assessed kidney exposure with a three-phase model consisting of a linear increase to the maximum within the initial minutes p.i., followed a bi-exponential decline. This three-phase-model served as reference for evaluating accuracy of dose estimates in 105 kidneys calculated by conventional mono-exponential fitting of the final three and four whole-body images.

**Results:** Mean effective half-life times for the reference model were  $25.8 \pm 12.0$  min and  $63.9 \pm 17.6$  h, predicting a mean renal dose of  $5.7 \pm 2.1$  Gy. The effective half-life time was  $46.3 \pm 15.4$  h for the last four and  $63.3 \pm 17.0$  h for the last three data points. The mean start of the first whole-body measurement was  $1.2 \pm 0.1$  h p.i. The ratio of fast to slow phases was  $28.1 \pm 23.9$  % at this time point, which caused a mean absolute percentage dose deviation of 12.4 % for four data points, compared to 3.1 % for three data points. At a mean time of 2.4 h p.i. (max 5.1 h), the ratio of fast to slow phase declined below 5 %.

**Conclusions:** Kinetic analysis of renal uptake using dynamic planar scans from the first hour after injection revealed a fast and a slow washout phase. Although the fast phase did not contribute substantially to the estimated renal dose, it could influence planar measurements performed within the first hours. We found that the presence of two clearance phases can hamper accurate dose estimation based on a single-phase model, resulting in approximately 12.4 % dose underestimation, thus potentially resulting in overtreatment. In the absence of dynamic initial recordings, the first dosimetry measurements should therefore be obtained later than 3–5 h after [ $^{177}\text{Lu}$ ]DOTATATE injection. Omitting the early whole-body image reduced the dose estimation error to 3.1 %.

**Key words:** Neuroendocrine tumor, Lutetium 177, Kidney dose, Dosimetry, Peptide receptor radionuclide therapy

---

## Introduction and Aim

Peptide receptor radionuclide therapy (PRRT) with radiolabeled somatostatin analogues has emerged as a well-established therapy option in the management of patients with metastasized neuroendocrine tumors (NETs) expressing somatostatin receptors, according to recently established guidelines [1, 2]. Currently, the most commonly used compounds are [ $^{90}\text{Y}$ ][DOTA<sup>0</sup>,Tyr<sup>3</sup>]octreotide ([ $^{90}\text{Y}$ ]DOTATOC) and [ $^{177}\text{Lu}$ ][DOTA<sup>0</sup>,Tyr<sup>3</sup>]octreotate ([ $^{177}\text{Lu}$ ] DOTATATE). Response to therapy is encouraging, with progression free survival of 33 months and overall survival rates up to 46 months [3, 4]. Although PRRT is well tolerated in most NET patients, and severe complications are rare, radiation toxicity remains a therapy-limiting factor. Whereas hematotoxicity is fortunately reversible in most cases, the kidneys are particularly at risk for overexposure [5, 6]. Cumulative dose values ranging from 23 to 29 Gy to the kidneys are reported as acceptable, in the absence of additional renal risk factors [7, 8].

PRRT with the beta- and gamma-emitting somatostatin analogue [ $^{177}\text{Lu}$ ]DOTATATE is accompanied with fewer side effects and yet equally successful therapy response rates as compared to [ $^{90}\text{Y}$ ]DOTATOC [3]. Furthermore, Lu-177 lends itself better for performing image-based dosimetric studies because of the gamma component, which allows simultaneous scintigraphy marking the beta treatment. Therapy is usually performed with standard doses of 7.4 GBq per cycle within four to six cycles [2]. Dose escalation and optimal patient-specific treatment informed by pre- and peri-therapeutic dosimetry findings, however, might enable maximal radiation dose to the tumors.

In general, the radiation exposures of the tumor and also the risk organs have to be monitored at intervals during the therapy so that total doses in the regions of interest can be calculated with some accuracy. A few well-selected time points must serve to this end, sparing the expense and effort entailed in collecting a prolonged series of measurements. In this regard, Larsson *et al.* [9] emphasized the importance of late time points for estimating radiation dose due to the long physical half-life of Lu-177. We now aim of optimizing clinical dosimetry with consideration of the influence of early time points on the estimation of kidney dose using a multi-phase kinetic model.

## Material and Methods

### *Patients and Therapy*

Patients with histologically proven well-differentiated metastatic NETs with expression of somatostatin receptors and a Ki-67 proliferation marker under 20 % were treated in multiple cycles with a default activity of 7.4 GBq [ $^{177}\text{Lu}$ ]DOTATATE per cycle. Labelling of the precursor DOTATATE (ABX GmbH, Radeberg, Germany) was performed according to the method described by

Breeman *et al.* [10] with slight modifications. The labelling with n.c.a. Lu-177 (ITG GmbH, Garching, Germany) was performed with 125  $\mu\text{g}$  peptide precursor in acetate buffer (pH 4.7). The radiochemical yield was greater than 95 % and the radiochemical purity greater than 98 % in the final preparation. For kidney dose estimation of one treatment cycle, we collected a sample of 64 (27 female, 37 male) consecutive patients (aged 62 $\pm$ 12 years; range 22–89 years). In some cases, more than one therapy cycle was used for the data analysis, resulting in a total of 105 datasets. The radiopharmaceutical was intravenously infused during 30 min at a rate of 1.6 ml/min. For prophylaxis against kidney damage, the i.v. administration of 1 l of an arginine and lysine solution (Pharmacy of the University Hospital of Munich, Germany) was initiated 30 min prior to the administration of the therapeutic (rate 5.8 ml/min).

### *Acquisition*

Prior to therapy, a diagnostic PET/CT scan (Biograph 64 TruePoint, Siemens Medical Solutions) using [ $^{68}\text{Ga}$ ]DOTATATE had been performed to locate the tumor metastasis and to quantify the maximum standardized uptake value (SUV<sub>max</sub>) of the tumor lesion.

For therapy monitoring and dosimetry estimation, distribution of the therapeutic agent [ $^{177}\text{Lu}$ ]DOTATATE was assessed dynamically with a dual-headed scintillation camera (E.cam, Siemens Medical Solution, 16 mm NaI(Tl) crystal) equipped with medium energy parallel hole collimators. Patients were positioned on the camera table in supine feet-first orientation. Detector heads were positioned in the anterior and posterior locations. An energy window was centered on the major gamma photon peak of the Lu-177 decay series (208 keV, width=15 %), together with additional windows (240 keV, width=10 %; 170 keV, width=15 %) to allow for scatter correction using the triple energy window method. Upon beginning the [ $^{177}\text{Lu}$ ]DOATATE infusion, a dynamic sequence of 12 planar frames (of 5 min each) was initiated in a 128 $\times$ 128 matrix of 4.8 mm pixels. Thereafter, whole-body images were acquired over 20 min in a 1024 $\times$ 256 matrix of 2.4 mm pixels at approximately 1, 24, 48, and 72 h post injection (or day 0, 1, 2, and 3 p.i.). An example series of posterior images is shown in Fig. 1.

The patient's urine was collected from a bladder catheter (female patients) or urine bottle (male patients) from the start of the infusion until the start of the first whole-body scan at approximately 1 h post injection to determine the net activity in the early images. For that purpose, the activity of 1-ml portions of the urine samples was measured with a high purity semi-conductor Germanium detector (Canberra Industries Inc. Model Gr0820) from which the total activity of the entire collected volume was calculated.

### *Planar Quantification*

Scatter correction was performed according to the triple energy window method described by Ichihara *et al.* [11]. For attenuation correction, the patient thickness and the kidney thickness were measured from the CT image, which had been obtained during diagnostic imaging. Furthermore, the kidney mass was determined for later dose calculations.

The activity  $A_j$  in a source region  $j$  was calculated according to Eq. 1. Attenuation correction was therein performed according to

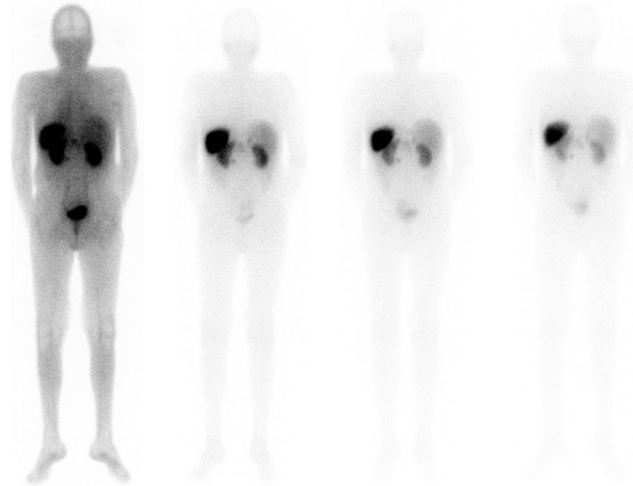


**Fig. 1** Posterior planar whole-body view approx. 1, 24, 48, and 72 h (from left to right) after administration of  $[^{177}\text{Lu}]\text{DOTATATE}$ .

the method published by Fleming *et al.* [12] and as suggested in the MIRD 16 Pamphlet [13] for isolated single source regions, with a correction for the source region attenuation  $f_j$  and the source thickness  $x_j$  with the coefficient  $\mu_j$ .

$$A_j = \sqrt{\frac{I_A I_P}{e^{-\mu_e x}}} \frac{(\mu_j x_j / 2)}{C \sinh(\mu_j x_j / 2)} = \sqrt{\frac{I_A I_P}{e^{-\mu_e x}}} \frac{f_j}{C} \quad (1)$$

where  $I_A$  and  $I_P$  are the counts per second (cps) detected in the anterior and posterior region of interest (ROI)  $j$ . The exponential term  $e^{-\mu_e x}$  represents the transmission factor for a patient with the total thickness  $x$  (cm) and with an individual attenuation value  $\mu_e$ . For the attenuation coefficients, we used the four component soft tissue values obtained from the XCOM cross section database [14].  $C$  is the calibration factor for each individual patient and therapy cycle in cps/Bq determined from the sum of counts in the first whole-body planar image, divided by the net remaining activity in this image.

To calculate the kidney counts, ROIs were drawn around the organ boundaries to scintigraphy, and attenuation corrected as described above. For background correction, an ROI was placed in an area without specific tracer accumulation, such as the lower abdomen or the thigh and subtracted with the method described by Kojima *et al.* [15] and presented in the MIRD 16 Pamphlet as “Background Subtraction: A Single Well-Defined Source Region Surrounded by Regions of Background Activity” to avoid over subtraction of background activity. Finally, the sum of counts from a whole-body ROI at day 0 were divided by the total administered activity, less the activity lost to micturition ( $1.3 \pm 0.5$  GBq, range 0.1–2.2 GBq). Only those organs without allocation of extra activity uptake due to overlay effects were analyzed; the right kidney was overlapped by liver activity in many projection images. Therefore, we decided to investigate solely the effect of early measurement time points for the left kidney. Patient data was excluded from this study when overlay of extrarenal activity was present in the images of the left kidney.

### Dose Calculations

The dose calculations in this work were performed according to the MIRD scheme [16]. The radiation dose is assessed by describing activity in source regions which irradiate target regions, as well as self-radiation of the target. The dose to a given target area is then calculated as the sum of all dose fractions from the source regions. To simplify the calculation, we assumed that most of the radiation damage to organs is caused by the beta radiation of Lu-177 and therefore neglected the irradiation by gamma-photons arising from other source regions. The mean absorbed dose  $D$  to the kidney was then calculated by:

$$D = \tilde{A} \times S \quad (2)$$

$\tilde{A}$  is the accumulated activity in the kidney (as a measure of all nuclear transitions) and  $S$  is the mean absorbed dose per unit accumulated activity (or the mean absorbed dose per nuclear transition). We applied a three-phase model (TrBi-exp) consisting of a linear increase to the maximum within the initial minutes of the infusion and a bi-exponential decline describing a rapid distribution phase and a slow washout/elimination phase. The bi-exponential function was fitted using the nonlinear least squares method in MATLAB (R2011a, The MathWorks, Inc.). To obtain the sum of all nuclear transitions, this three-phase model was integrated over time to infinity. The cumulated activity  $\tilde{A}$  was then used to estimate the absorbed dose  $D$  together with the kidney-specific  $S$  value for Lu-177 obtained from the RADAR website [17]. A rescaling to the individual patient kidney mass was performed according to [18]

$$S(\text{patient}) = S(\text{MIRD}) \frac{m(\text{MIRD})}{m(\text{patient})} \quad (3)$$

using the MIRD mass and  $S$  values from the kidneys of the adult phantoms [19].

## Investigating the Effect of Early Time Points

The integrated activity of TrBi-exp served as baseline for evaluating kidney doses calculated from four whole-body static images at approx. 1, 24, 48, and 72 h p.i. (4P-fit) or only the last three whole-body images (3P-fit). We compared a mono-exponential function with two parameters

$$f_0(t) = p_1 e^{-p_2 t} \quad (4)$$

as the null hypothesis, with a set of three-parametrical fit functions as the alternate hypothesis, with fit parameters  $p_i$  and—in the case of Eq. 5b as in [20, 21]—with a separate consideration of the physical decay constant  $\lambda_{\text{phys}}$

$$f_1(t) = p_1 \left( e^{(-p_2 t)} + e^{(-p_3 t)} \right) \quad (5a)$$

$$f_2(t) = p_1 e^{-(p_2 + \lambda_{\text{phys}})t} + p_3 e^{-\lambda_{\text{phys}} t} \quad (5b)$$

The most appropriate model  $f_m$  (with  $m$  being 0, 1, or 2, as defined in equations 4 and 5) was then chosen by performing the  $F$  test [20]. For the null hypothesis (null) and the alternative hypothesis (alt), the squares of the residuals between fitted model and measured data points were summed yielding  $SSR_{\text{null}}$  and  $SSR_{\text{alt}}$ . The corresponding degrees of freedom,  $DF_{\text{null}}$  and  $DF_{\text{alt}}$ , were calculated by subtracting the number of fit parameters from the number of available measurement points. The  $F$  value was then obtained by:

$$F = \frac{(SSR_{\text{null}} - SSR_{\text{alt}}) DF_{\text{alt}}}{(DF_{\text{null}} - DF_{\text{alt}}) SSR_{\text{alt}}} \quad (6)$$

If the  $p$  value was under the significance level of  $\alpha=0.05$ , the null hypotheses was rejected, and the alternate model was used. The corrected Akaike Information Criterion (AICc), which is proposed by Glatting *et al.* [20] and Kletting *et al.* [22], is not here feasible, since AICc requires at least three more data points than the number of parameters. For the case of the 3P-fit, we used the mono-exponential function (Eq. 4) with two parameters to increase the probability for successful fitting of noisy data by providing a model which has fewer fit parameters than the number of available data points. Using the model  $f_m$  which was selected by the  $F$  test for each individual patient  $j$ , we then determined the percentage deviation of the accumulated activity  $\tilde{A}_{m,j}$  relative to the accumulated activity  $\tilde{A}_{\text{TrBi},j}$  of the baseline model TrBi-exp:

$$\%DEV_j = \frac{\tilde{A}_{m,j} - \tilde{A}_{\text{TrBi},j}}{\tilde{A}_{\text{TrBi},j}} \times 100 \quad (7)$$

Thus, a negative %DEV would indicate underestimation and a positive %DEV overestimation of the real dose. We calculated the corresponding mean deviation from baseline for all  $n$  patients using the appropriate model  $f_m$  for each patient  $j$  as selected by the  $F$  test:

$$M = \frac{1}{n} \sum_{j=1}^n |\%DEV_j| = \frac{1}{n} \sum_{j=1}^n \left| \frac{\tilde{A}_{m,j} - \tilde{A}_{\text{TrBi},j}}{\tilde{A}_{\text{TrBi},j}} \right| \times 100 \quad (8)$$

## Results

### Calculated Dose with TrBi-exp

All bi-exponential curve fits succeeded, with a mean coefficient of determination ( $R^2$ ) value of  $0.995 \pm 0.010$  and minimum  $R^2$  of 0.973. Data for a representative kidney time activity curve is shown in Fig. 2, with the bi-exponential fit in green. This bi-exponential consists of two phases, which can interfere during the first hours. The population mean effective half live  $T_{1/2}$  was  $25.8 \pm 12.0$  min for the fast phase and  $63.9 \pm 17.6$  h for the slow phase. Using the TrBi-exp model, the mean calculated dose of all 105 patient datasets was  $5.7 \pm 2.1$  Gy (range 2.5–13.8 Gy), which gave a mean kidney dose of  $0.8 \pm 0.3$  Gy/GBq administered. Because TrBi-exp is a linear combination of three functions, the mean dose factors and the percentage contribution to the total dose can be specified separately (Table 1). The kidney masses used for mass correction of the  $S$  values according to Eq. 3 ranged from 104 to 396 g, with a mean value of  $186 \pm 45$  g.

### Dosimetry Using Four Whole-Body Planar Image Time Points (4P-fit)

Before calculating the accumulated activity from only four late scintigraphy measurements, the best fitting of a set of models was chosen with the  $F$  test, as described above. In five of 105 cases, the model  $f_1$  (Eq. 5a) was favored instead of the mono-exponential function, for which an example is shown in Fig. 3a. In this graph, the bi-exponential part of the baseline function (green), mono-exponential (cyan) and  $f_1(t)$  (purple) functions are visualized. In most cases, the alternative models were rejected, as illustrated in Fig. 3b, where the baseline (green) and the mono-exponential (cyan) fits are plotted together with the fits onto model  $f_1(t)$  (purple). Using the matching fit model for each kidney the mean  $R^2$  was  $0.965 \pm 0.032$  for the 4P-fit. Analyzing the fit parameters indicated an initial mean activity from parameter  $p_1$  in the kidneys of  $153.8 \pm 56.1$  MBq (range 71–389 MBq). For the slow washout parameter, the mean half-life for 4P-fit was  $46.3 \pm 15.4$  h (range 21.5–90.5 h). The calculated dose with these parameters was  $5.0 \pm 1.9$  Gy (range 2.5–11.3 Gy).

### Dosimetry Using 3 Whole-Body Planar Image Time Points (3P-fit)

Omitting the first measurement point at approx. 1 h p.i. and using the mono-exponential fit (3P-fit), the mean  $R^2$  was  $0.983 \pm 0.030$ . Analysis of the fit parameters indicated a mean initial activity of  $126.5 \pm 39.2$  MBq (range 45–258 MBq) in the kidneys and a mean effective half-life of  $63.3 \pm 17.0$  h (range 34.1–115.1 h). The resulting mean dose was  $5.6 \pm 2.1$  Gy (range 2.5–14.1 Gy).

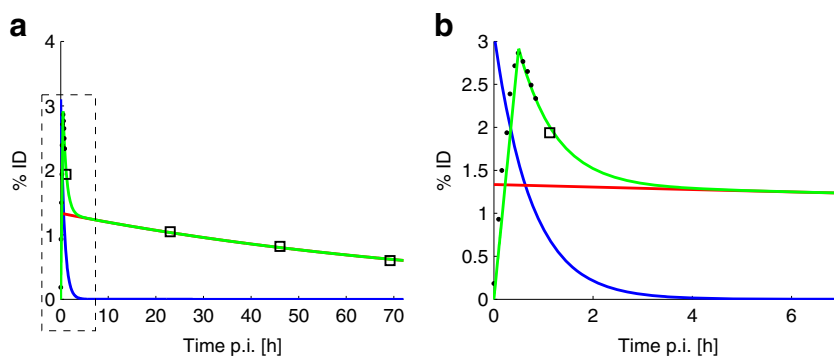


**Fig. 2** **a** Time activity curve of the left kidney of a patient with dynamic planar measurement of [ $^{177}\text{Lu}$ ]DOTATATE within the first hour (*filled circles*) and planar whole body scintigraphies up to 70 h post injection (*open squares*). The bi-exponential fit is plotted in green and its two exponentials, which represent the different phase fractions, are plotted in *blue* (fast;  $T_{1/2}=31$  min) and *red* (slow;  $T_{1/2}=63$  h). **b** This plot focuses on the early phase within the first 6 h indicated by the *dashed rectangular area* in (**a**) so as to visualize the linear increase to the maximum within the initial minutes of the infusion.

### Comparison of Dose Estimation Approaches with Baseline

The deviation of the dose calculated with 3P-fit (blue) and 4P-fit (red) from the dose calculated with TrBi-exp is presented for each of the 105 kidneys in Fig. 4a. In only 7 of 105 datasets was the absolute deviation from the calculated dose higher when the first measurement point was omitted. We saw a maximum absolute deviation of 41.1 % with the 4P-fit compared to a maximum of 13.8 % with 3P-fit, calculated relative to the baseline method. The mean absolute percentage deviation was  $12.4\pm 9.2$  % with four points and  $3.1\pm 2.5$  % with three points. With the exception of six patients, the calculated dose with four points was always underestimated, whereas the calculation with three time points underestimated dose in 65 and overestimated in 40 cases. Calculated doses of the baseline model TrBi-exp, 4P-fit, and 3P-fit are shown in Fig. 4b. The mean dose value with four late points was significantly decreased compared to the other two methods.

## Discussion

Considering the generally impaired health status of most patients undergoing PRRT, it is mandatory to obtain reliable dosimetric data with a minimal number of measurements. As in previous dosimetry investigations [23–25], we decided to conclude dosimetry monitoring at 72 h because of logistic reasons. This work is based on the assumption that all kinetic models are valid beyond the last data point at 72 h p.i. Although we have no proof that this assumption holds,

others who had measurements available over a longer time interval, e.g., until approximately 168 h [9, 26, 27], have not observed a deviation of data and exponential model at later times. We therefore assume that the models utilized in this work are suitable descriptions for estimation of the kidney dose. The contribution of the first 72 h to the kidney dose calculated using our proposed reference model TrBi-exp was approximately  $54.6\pm 9.2$  % (range 34.1–73.7 %).

The limitation to planar scintigraphies is a potential weakness of this study since quantitation of planar scintigraphy is subject to several caveats arising from attenuation and overlap of tissues. Especially, uncertainties due to overlap could be prevented, and radionuclide concentration calculations could be improved by performing 3D dosimetry based on quantitative SPECT/CT measurements [27]. Recent SPECT/CT studies utilizing the radionuclide Lu-177 reported encouraging accuracies and methods in quantitative imaging [28, 29]. The patient group in this study was pre-selected to contain no obvious kidney overlay in the planar images; therefore, we did not expect a major influence of superpositioned organs. Dosimetry from SPECT/CT images will be addressed in future investigations.

In this paper, we studied the effect of reducing the number of time samples on the outcome of the dosimetry calculations, based on various kinetic models and truncation of the data to as few as three time points. Present data show that the concentration of radioactivity derived from [ $^{177}\text{Lu}$ ]DOTATATE in the kidneys is not well described using a single exponential function; we tested several simple multi-phase models, the best of which proved to be a model composed of three phases. Here, the fast initial uptake phase

**Table 1.** Absolute and relative contribution of the single phases to the total dose function TrBi-exp. Each value was obtained from 105 kidneys

Function	Mean [Gy]	SD [Gy]	Min. [Gy]	Max. [Gy]	Rel. [%]
Linear phase	0.03	0.01	0.01	0.08	0.6
Fast phase	0.03	0.03	0.003	0.19	0.6
Slow phase	5.6	2.1	2.5	13.8	98.9
TrBi-exp (all)	5.7	2.1	2.5	13.8	100

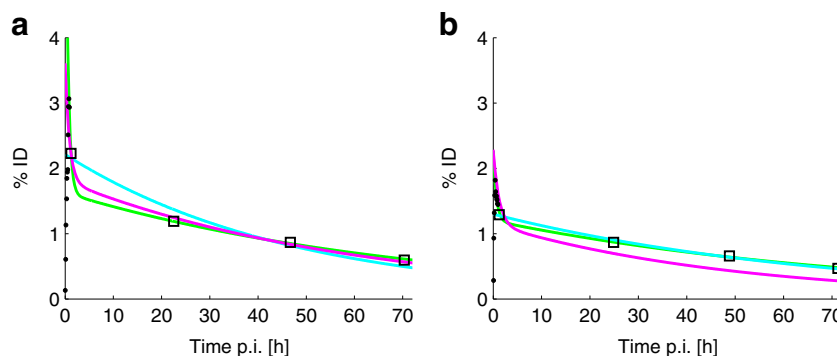


**Fig. 3** Example of fit models with four static planar kidney measurement points. **a** The mono-exponential fit is plotted in cyan ( $R^2=0.968$ ) and function  $f_1(t)$  (Eq. 5a) is plotted in purple ( $R^2=0.997$ ). The  $F$  test indicated  $f_1(t)$  to be superior in this case ( $P<0.025$ ). For comparison, TrBi-exp is plotted in green. **b** A representative patient in whom the  $F$  test rejected  $f_1(t)$ . Here, the mono-exponential fit (cyan;  $R^2=0.994$ ) was superior to the model  $f_1(t)$  (Eq. 5a,  $R^2=0.541$ ).

was described by a linear increase from time 0 to the time of maximum tracer concentration in the kidneys and was followed by a linear combination of two exponential functions, representing phases of elimination with different time characteristics. For the group of patients, this model gave mean effective half-lives of  $25.8\pm 12.0$  min for the fast phase and  $63.9\pm 17.6$  h for the slow phase. In pharmacokinetic studies, such results are generally interpreted to reveal a distribution phase followed by a slow elimination phase. Comparing the mean relative contributions to the total absorbed dose (Table 1), we found that almost the entire dose (98.9 %) is attributable to the slow phase component. The mean dose values for the left kidney per therapy cycle were  $5.7\pm 2.1$  Gy ( $0.8\pm 0.3$  Gy/GBq), which is in good accordance to previous studies [26, 30, 31]. In agreement with Sandstroem *et al.* [27] and others [32], we noticed a wide range of kidney doses (2.5–13.8 Gy; median 5.3 Gy), likely reflecting a wide range of renal absorption and elimination parameters of the multi-phase kidney activity kinetics in this heterogeneous population. The occurrence of this observed dose variation, where individuals at the high end might easily encounter radiotoxicity, substantiates the need for an individualization of the peptide radionuclide receptor therapy.

A systematic analysis of the observed multi-phase model yielded the following results; based on earlier reports [13, 27], we at first expected an overall higher dose if the first data point was measured during the fast elimination phase. Comparing the mean initial activities in the kidney from 4P-fit ( $153.8\pm 56.1$  MBq) and 3P-fit ( $126.5\pm 39.2$  MBq), indicated a 21.3 % higher calculated dose, as expected for the 4P-fit. Comparing the time activity curve of one representative patient's dataset (Fig. 5) indicated a considerable overestimation of initial uptake, propagating to an artifact of increased area under the curve within the first days after treatment. However, we also observed a steeper descent of the exponential curve caused by the elevated first data point, which led to systematic underestimation of the half-life of the exponential. Hence, when integrating these exponentials to infinity, the area under the entire curve (*i.e.*, the total dose) would consequently be substantially smaller than as predicted by the baseline or the 3P-fit models. Consequent underestimation of the total calculated dose is illustrated by comparison of Fig. 4.

This finding is in concordance with the earlier observations of Guerriero *et al.* [23], who also investigated the accuracy of estimated dose when certain data points were omitted. Their remarks on the inadequate number of

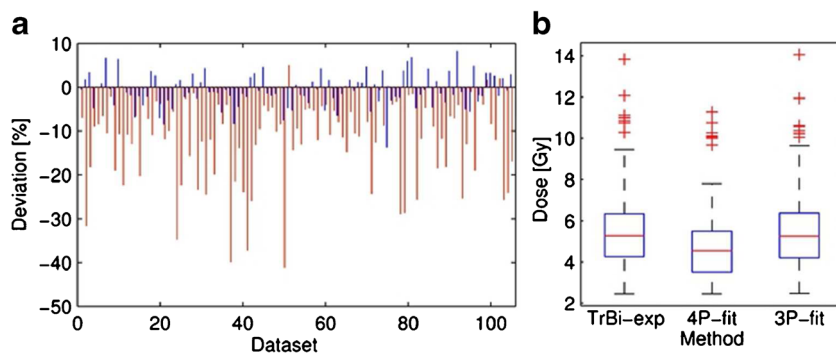


**Fig. 4** **a** Comparison of the percentage deviation to TrBi-exp with all four planar measurement time points (4P-fit; red) or only the last three planar measurement points (3P-fit; blue) of all 105 patient datasets. A positive value indicates an overestimation and a negative value an underestimation of the dose. **b** Boxplots of the dose calculated with TrBi-exp (left), 4P-fit (middle), and 3P-fit (right). Outliers are plotted individually (red).

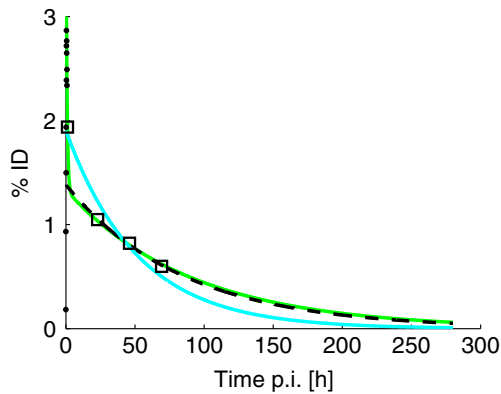


**Fig. 5** Comparison of fits of planar scintigraphy data with four points (4P-fit, cyan), 3 points (3P-fit, dashed black), and the bi-exponential fit (Bi-exp, green) including the dynamic data during the first 30 min after infusion. The abscissa was extended to distinguish the gradients of the curves.

available data points to describe multiple phases arose from SPECT images at comparable time points as in the present work, except that no dynamic sampling of the initial fast phase was available to them. Provided with the initial dynamic data, we concur with their observations. Furthermore, our data allow us to describe the fast and slow phases separately and predict a time point after which the influence of the fast phase onto the overall time activity curve diminishes. In contrast to [9], where kidney dose was assessed by four planar images during days 0, 1, 2, and 7, we did not observe peak activities in the kidneys at day 1 or later. Omitting the late day 7, data point had a noticeable effect on the estimated kidney dose in their work. As this situation is similar to using the 4P-fit in our present work but with day 2 constituting the latest time point, our findings indicate that this effect may rather be related to the mixture of the fast and slow retention phases in the early data points, but in concordance with [9], the effect could be weakened when data points later than day 3 are included.

To study the fast-phase influence on the day 0 whole-body image in some detail, we calculated the ratio between fast and slow phases from the bi-exponential model. The mean time of the first whole-body measurement was  $1.2 \pm 0.1$  h after injection, when the mean relative ratio between the fast and slow phases was  $28.1 \pm 23.9$  %. The mean time point at which this ratio fell below an arbitrary value of 5 % was 2.4 h p.i. (max 5.1 h), whereupon the contribution of the first phase might safely be ignored. Figure 6 illustrates the effect on treatment day 0 of this influenced measurement onto the percentage dose deviation (compared to TrBi-exp), when the total dose was calculated with (4P-fit, red) or without (3P-fit, blue) the day 0 measurement. The Spearman's test gave  $\rho$  of 0.91 (4P-fit), indicating a very strong correlation between the dose deviation and the contribution of the fast retention phase to the day 0 measurement. In the case of the three time points (3P-fit), no such correlation was found ( $\rho=0.01$ ).

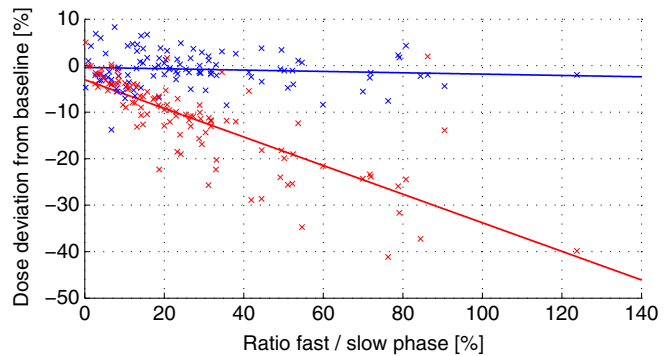


**Fig. 6** Percentage dose deviation compared to the baseline function TrBi-exp with four time points (red) and the last three time-points (blue) as functions of the ratio of fast to slow phases at the first whole-body measurement day. A linear regression is shown for both cases.

The coefficient of determination  $R^2$  of the 4P-fit was consistently high (circa 0.97), which would not in itself alert to this bias. Nevertheless, the utilization of more sophisticated fitting algorithms, which assign individual weights to each measurement point, is certainly sufficient to reduce the mismatch between treatment day measurements and the chosen mono-exponential kinetic model. Our observations confirm that high  $R^2$  values cannot be relied upon as proof of model fitness but that curve fits should be carefully checked by an experienced reader. This is illustrated in Fig. 5, where the 4P-fit results in  $R^2$  of 0.95, although this fit clearly does not represent the true situation. The inadequacy of  $R^2$  as an indicator for the fit quality of nonlinear functions is in accordance with Spiess *et al.* [33]. When the same model is applied to only a subgroup of these data, *i.e.*, omitting the treatment day whole-body scan, the accuracy of the results could be significantly improved. Nevertheless, limitations could arise from this reduction of data especially if one of the remaining measurements is not available due to a hardware failure or patient discomfort. It is generally understood that at least three data points are needed for modelling an exponential phase, as noted by Lassmann *et al.* [34].

A mean dose deviation from the 4P-fit of  $12.4 \pm 9.2$  % in a single therapy cycle is unlikely to be a factor in the risk for radiation-induced nephropathy. However, an accumulation of such dose underestimations in multiple therapy cycles could well lead to a substantial and relevant underestimation of total radiation dose to the kidneys. In three of 105 individual cases, we observed a dose deviation for the 4P-fit of up to 40 %, corresponding to 3 Gy in a single cycle (see Fig. 4a). In seven of 105 datasets, the underestimation exceeded 2 Gy. If dose estimates from individuals are used for designing dosimetry-supported individualized therapies, the observed underestimations would cause ill-planning of therapeutic doses of subsequent cycles. Hence, the risk of receiving a critically high radiation dose increases significantly for patients across the treatment cycle.

## Conclusion and Outlook

We studied the effect of reducing the number of measurement times on the outcome of dosimetry calculations based on various multi-phase descriptions of the kidney activity following a [ $^{177}\text{Lu}$ ]DOTATATE treatment cycle in a series of 64 NET patients. We found that the majority of the kidney dose occurs during the slow washout phase, which is integrated to infinity, as in conventional pharmacokinetic models. We also found that interference of early measurements by the fast washout phase biases the results, sometimes resulting in severe underestimation of the kidney dose. This work demonstrates that the accuracy of dosimetric values for the kidneys largely depends on a proper determination of the slow phase for renal washout. However, careful selection of data points avoids errors arising from integration of unsuitable early data, which may be affected by the fast phase. These observations support reducing the number of scintigraphy measurements without compromising the accuracy of image-based dosimetry. These findings should facilitate optimized dosimetry scanning protocols, while minimizing the work load for staff and patients. Scintigraphy results may generalize to quantitative SPECT measurements, which are not dependent on the whole-body calibration. Thus, we recommend starting the first dosimetric measurement 24 h after radiotherapeutic agent injection.

*Acknowledgments.* The authors would like to thank the colleagues from the Department of Nuclear Medicine for their participation in data collection. Especially, we would like to thank the nuclear medicine technicians for performing the imaging studies and the nurses of the nuclear medicine therapy ward for urine collection. We note professional editing of the manuscript provided by Inglewood Biomedical Editing.

*Conflict of Interest.* The authors declare that they have no conflict of interest.

*Human Rights Statement.* For this type of study, formal consent is not required.

## References

- Pavel M, Baudin E, Couvelard A et al (2012) ENETS consensus guidelines for the management of patients with liver and other distant metastases from neuroendocrine neoplasms of foregut, midgut, hindgut, and unknown primary. *Neuroendocrinology* 95:157–176
- Bodei L, Mueller-Brand J, Baum RP et al (2013) The joint IAEA, EANM, and SNMMI practical guidance on peptide receptor radionuclide therapy (PRRT) in neuroendocrine tumours. *Eur J Nucl Med Mol Imaging* 40:800–816
- van der Zwan WA, Bodei L, Mueller-Brand J, et al. (2014) GEP-NETS update: radionuclide therapy in neuroendocrine tumors. *European journal of endocrinology / European Federation of Endocrine Societies*
- Koch W, Auernhammer CJ, Geisler J et al (2014) Treatment with octreotide in patients with well-differentiated neuroendocrine tumors of the ileum: prognostic stratification with Ga-68-DOTA-TATE positron emission tomography. *Mol Imaging* 13:1–10
- Bodei L, Cremonesi M, Grana CM et al (2012) Yttrium-labelled peptides for therapy of NET. *Eur J Nucl Med Mol Imaging* 39(Suppl 1):S93–S102
- Kam BL, Teunissen JJ, Krenning EP et al (2012) Lutetium-labelled peptides for therapy of neuroendocrine tumours. *Eur J Nucl Med Mol Imaging* 39(Suppl 1):S103–S112
- Konijnenberg M, Melis M, Valkema R et al (2007) Radiation dose distribution in human kidneys by octreotides in peptide receptor radionuclide therapy. *J Nuclear Med : Off Public Soc Nuclear Med* 48:134–142
- Emami B, Lyman J, Brown A et al (1991) Tolerance of normal tissue to therapeutic irradiation. *Int J Radiat Oncol Biol Phys* 21:109–122
- Larsson M, Bernhardt P, Svensson JB et al (2012) Estimation of absorbed dose to the kidneys in patients after treatment with  $^{177}\text{Lu}$ -octreotate: comparison between methods based on planar scintigraphy. *EJNMMI Res* 2:49
- Breeman WA, De Jong M, Visser TJ et al (2003) Optimising conditions for radiolabelling of DOTA-peptides with  $^{90}\text{Y}$ ,  $^{111}\text{In}$  and  $^{177}\text{Lu}$  at high specific activities. *Eur J Nucl Med Mol Imaging* 30:917–920
- Ichihara T, Ogawa K, Motomura N et al (1993) Compton scatter compensation using the triple-energy window method for single- and dual-isotope SPECT. *J Nuclear Med : Off Public Soc Nuclear Med* 34:2216–2221
- Fleming JS (1979) A technique for the absolute measurement of activity using a gamma camera and computer. *Phys Med Biol* 24:176–180
- Siegel JA, Thomas SR, Stubbs JB et al (1999) MIRDO pamphlet no. 16: techniques for quantitative radiopharmaceutical biodistribution data acquisition and analysis for use in human radiation dose estimates. *J Nuclear Med : Off Public Soc Nuclear Med* 40:375–615
- Berger MJ, Hubbell JH, Seltzer SM (2010) XCOM: photon cross section database (version 1.5). <http://physics.nist.gov/xcom>. National Institute of Standards and Technology, Gaithersburg
- Kojima A, Takaki Y, Matsumoto M et al (1993) A preliminary phantom study on a proposed model for quantification of renal planar scintigraphy. *Med Phys* 20:33–37
- Loevinger R, Berman M (1968) A formalism for calculation of absorbed dose from radionuclides. *Phys Med Biol* 13:205–217
- Stabin M, Siegel J, Hunt J et al (2001) RADAR: the radiation dose assessment resource. *J Nucl Med* 42
- Williams LE, Liu A, Yamauchi DM et al (2002) The two types of correction of absorbed dose estimates for internal emitters. *Cancer* 94:1231–1234
- Stabin MG, Xu XG, Emmons MA et al (2012) RADAR reference adult, pediatric, and pregnant female phantom series for internal and external dosimetry. *J Nuclear Med : Off Public Soc Nuclear Med* 53:1807–1813
- Glatting G, Kletting P, Reske SN et al (2007) Choosing the optimal fit function: comparison of the Akaike information criterion and the F-test. *Med Phys* 34:4285–4292
- Kletting P, Schimmel S, Kestler HA et al (2013) Molecular radiotherapy: the NUKFIT software for calculating the time-integrated activity coefficient. *Med Phys* 40:102504
- Kletting P, Kull T, Reske SN, Glatting G (2009) Comparing time activity curves using the Akaike information criterion. *Phys Med Biol* 54:N501–N507
- Guerrero F, Ferrari ME, Botta F et al (2013) Kidney dosimetry in (1)(7)(7)Lu and (9)(0)Y peptide receptor radionuclide therapy: influence of image timing, time-activity integration method, and risk factors. *BioMed Res Int* 2013:935351
- Baechler S, Hobbs RF, Prideaux AR et al (2008) Extension of the biological effective dose to the MIRDO schema and possible implications in radionuclide therapy dosimetry. *Med Phys* 35:1123–1134
- Cremonesi M, Botta F, Di Dia A et al (2010) Dosimetry for treatment with radiolabelled somatostatin analogues. a review. *Quart J Nuclear Med Molec Imag : Off Public Italian Assoc Nuclear Med* 54:37–51
- Garkavij M, Nickel M, Sjogreen-Gleisner K et al (2010)  $^{177}\text{Lu}$ -[DOTA $^0$ , Tyr $^3$ ] octreotate therapy in patients with disseminated neuroendocrine tumors: analysis of dosimetry with impact on future therapeutic strategy. *Cancer* 116:1084–1092
- Sandstrom M, Garske U, Granberg D et al (2010) Individualized dosimetry in patients undergoing therapy with (177)Lu-DOTA-D-Phe (1)-Tyr (3)-octreotate. *Eur J Nucl Med Mol Imaging* 37:212–225
- Beauregard JM, Hofman MS, Pereira JM et al (2011) Quantitative (177)Lu SPECT (QSPECT) imaging using a commercially available SPECT/CT system. *Cancer Imag : official Public Int Cancer Imag Soc* 11:56–66
- Sanders JC, Kuwert T, Hornegger J, Ritt P (2014) Quantitative SPECT/CT Imaging of Lu with *in vivo* validation in patients undergoing peptide receptor radionuclide therapy. *Molec Imag Biol: MIB : Off Public Acad Molec Imag*
- Kwekkeboom DJ, Bakker WH, Kooij PP et al (2001) [ $^{177}\text{Lu}$ -DOTA $^0$ Tyr $^3$ ]octreotate: comparison with [ $^{111}\text{In}$ -DTPA $^0$ ]octreotide in patients. *Eur J Nucl Med* 28:1319–1325



31. Wehrmann C, Senfleben S, Zachert C et al (2007) Results of individual patient dosimetry in peptide receptor radionuclide therapy with  $^{177}\text{Lu}$  DOTA-TATE and  $^{177}\text{Lu}$  DOTA-NOC. *Cancer Biother Radiopharm* 22:406–416
32. Helisch A, Forster GJ, Reber H et al (2004) Pre-therapeutic dosimetry and biodistribution of  $^{86}\text{Y}$ -DOTA-Phe1-Tyr3-octreotide *versus*  $^{111}\text{In}$ -pentetreotide in patients with advanced neuroendocrine tumours. *Eur J Nucl Med Mol Imaging* 31:1386–1392
33. Spiess AN, Neumeyer N (2010) An evaluation of  $R^2$  as an inadequate measure for nonlinear models in pharmacological and biochemical research: a Monte Carlo approach. *BMC Pharmacol* 10:6
34. Lassmann M, Chiesa C, Flux G et al (2011) EANM dosimetry committee guidance document: good practice of clinical dosimetry reporting. *Eur J Nucl Med Mol Imaging* 38:192–200